1

Vortices in resonant polariton condensates in semiconductor microcavities

D. N. Krizhanovskii, K. Guda, M. Sich, M. S. Skolnick
Department of Physics and Astronomy, the University of Sheffield, Sheffield, S3 7RH, United Kingdom

L. Dominici, D. Sanvitto
NANOTEC, Istituto di Nanotecnologia — CNR, Via Arnesano, 73100 Lecce, Italy

Abstract

We review studies of quantised vortices in polariton condensates in three main configurations, namely offresonant, optical parametric oscillator OPO and direct resonant excitation. A brief introduction is given on the typical interferometric detection and spinor nature of polaritons. Specific experiments are described in details, highlighting the dynamics of spontaneous and imprinted vortices in OPO and resonant polariton condensate, and the role of nonlinearities. Time-resolved measurements reveal metastable rotational polariton flow indicating superfluid-like behaviour. In the case of a ring-shaped pump, a transition from the vortex state with angular momentum $M = 1$ to $M = 2$ is observed due to interplay between gain and polariton-polariton interactions. Finally, we demonstrate the direct pulsed initialization of a condensate carrying an half-vortex, and the spontaneous creation of vortices when starting from ring-shaped condensates. These are created in vortex – anti-vortex pairs due to the interplay between breaking of $y \mapsto -y$ reflection symmetry in the system and conservation of orbital angular momentum.

1.1 Introduction

Coherent macroscopically occupied states (condensates) attract major interest since they exhibit a number of interesting phenomena, such as superfluidity, vortices and solitons. As well as coherent condensates of liquid helium and dilute atomic gases, condensates of semiconductor microcavity polaritons constitute an appealing testbed allowing easy optical manipulation and direct imaging of the condensate due to the photonic part of their hybrid light-matter wave-function[1, 2]. In contrast to the atomic BEC the

polariton system is a non-equilibrium system[3], where a dynamic balance between loss and gain from an external pump field is formed. Furthermore, polaritons also have strong nonlinearities while their spinor nature allows for half-integer vorticity.

In this chapter, we review the main obervations of polariton vortices and also describe some specific experiments more in detail. In the first paragraphs, we give an introduction to the quantised vortices in condensates, how they can be recognized using interferometric detection, and to the spinor nature of polaritons. We briefly discuss spontaneous generation of vortices under nonresonant excitation. Then we consider non-equilibrium polariton condensates arising from polariton-polariton parametric scattering into macroscopically occupied signal at $k_s \sim 0$ and idler states at $k_i \sim 2k_p$ for resonant pump excitation into the lower polariton branch at $k = k_p$. This regime corresponds to the so-called optical parametric oscillator (OPO, see Figure 1.3(a)), which has attracted significant interest [4, 5]. Importantly, the phase of the signal is not imprinted by the pump but forms spontaneously due to $U1$ symmetry breaking as in the case of incoherently pumped condensates[6]. The OPO system consists of three macroscopically occupied coherently coupled signal, pump and idler states and hence is more complicated than a single resonant fluid or nonresonatly pumped condensate. In this chapter we mainly focus on the properties of vortices in the signal condensate and how these are affected by the pump and idler. Finally, a description of some main experiments in the case of resonant excitation at $k = 0$ is presented, comprising the case of a direct imprint of a polariton condensate with the topological charge of a full or half-vortex.

The phenomenology of spontaneous pattern formation is much richer in non-equilibrium than in equilibrium systems [7], with vortices being a typical example. Vortices are topological defects occurring in optics and condensed matter as well as in particle physics and cosmology. In vortices in quantum fluids the phase of a field winds around vortex core where the density is almost zero with a change for a complete loop being an integer multiple of 2π. Therefore, a vortex can be described by a state with quantised orbital angular momentum (OAM), also said phase winding. In optics this degree of freedom can be further used in photonic quantum information applications and also polariton vortices have been proposed for information processing [8].

Atomic Bose-Einstein condensates [9], liquid helium [10] and semiconductor lasers [11] (VCSELs) exhibit formation of vortices. In equilibrium systems such as a BEC of cold atoms or liquid helium the existence of stable vortex is a manifestation of superfluidity. In nonequilibrium systems, like non-resonant incoherently pumped polariton condensate in CdTe microcav-

ities, spontaneous vortices may form due to the interplay between polariton flows and natural photonic potential disorder, e.g. localized defects [12]. Half-vortices, where only one spin (or circular polarisation, which is associated to SAM, spin angular momentum) component of the condensate exhibits a vortex can be also observed [13]. It is important that the excitonic component in the polariton wavefunction leads to very strong polariton-polariton interactions and consequently to a giant $\chi^{(3)}$ optical nonlinearity, which affect the vortex formation as discussed in the manuscript. These very strong interactions also enable observation of effects such as bright solitons [14, 15] or polariton superfluidity at very moderate particle densities. Vortices can be generated in polariton superfluids flowing against an obstacle as a result of oblique dark solitons breaking into streets or trains of vortex - anti-vortex pair at subsonic critical velocities of the quantum fluid [16, 17].

The aim of this chapter is to describe several experimental results showing the effect of interactions and of the nonequilibrium polariton nature on the formation and dynamics of polariton vortices in OPO and resonant condensates. Firstly, we demonstrate that vortices in a polariton condensate can be created using a weak external imprinting beam (which we term the *im*-beam). The vortex core radius is determined by polariton-polariton interactions leading to a decrease of the vortex radius with increasing particle density [18]. It is shown that OAM is conserved during pair polariton-polariton scattering and hence the imprinting of vortices on the signal state is accompanied by formation of an antivortex in the corresponding idler state [18]. The measurements of temporal evolution of an imprinted vortex reveal metastable polariton flow consistent with a superfluid-like behaviour of the interacting polariton system. Secondly, we show that vortices may arise spontaneously in an artificially created potential landscape [19]. The optically induced potential can be created by a ring-shaped pump beam, carrying zero orbital angular momentum (OAM). The formation of a stable vortex with OAM $M = 1$ is observed due to breaking of the $y \mapsto -y$ reflection symmetry of the system. At higher excitation density the interplay between the kinetic energy of the vortex due to localisation, the potential interaction energy within the condensate and the spatial distribution of the gain results in spontaneous formation of a vortex with OAM $M = 2$. Finally, we investigated vortices in an artificial condensate injected directly at $k = 0$ by a pulsed pump beam [19]. One powerful tool of the resonant scheme is that it allows to create the condensate directly with an initial full or half-vortex topological charge and to follow their evolution in different regimes. Also, it is possible to start with a zero-winding state but with a space inhomogeneous profile, in order to induce and observe the formation

of a vortex – anti-vortex pair, dictated by the conservation of OAM. All the experiments were performed at 4 K. The detailed description of the GaAs-based microcavity samples and experimental techniques can be found in Refs. [18, 19].

1.2 Signature of vortex in interference and phase maps

One useful characteristic of polariton condensates is their hybrid photonic-electronic nature, which continuously emits photons coherently with the condensate wavefunction. In this sense not only imaging of the fluid is possible, but also of the phase of their complex wavefunction. This can be retrieved when letting the emission from the fluid to interfere with a coherent wave: two major cases are possible. One, the emission from a fluid which is created by nonresonant excitation (and hence becomes noncoherent with the excitation beam), has to be let auto-interfere with itself, either with a centre- or axis-symmetric copy of the emission image, or with an expanded and homogeneous portion of the same field. This also allows time-resolved measures of the emission provided the coherence time is long enough, while the time resolution is limited by the emission duration itself. Two, the emission from a resonantly excited polariton fluid, can be let interfere instead with the original exciting pulse, which is possible and indeed typical only for the resonant excitation scheme and not for the offresonant one. Here the time resolution is given by the pulse width. In both cases, signature of a vortex is seen by typical patterns in the interferograms: a fork-like dislocation with an excess number of fringes on one side equal to the quantised charge of the vortex M. Here we show in Figure 1.1 an exemplificative case of the vortex recognition scheme for a resonant OPO vortex, where panel (a) is the intensity map and (b) the interferogram (extracted from [20]).

Typically such images are used, together, to report on the observation, formation and motion of quantised vortices. A further possible step, is to use digital holographic technique, i.e., Fourier analysis, to retrieve maps of the phase distribution of the fluid, as in panel (c). These show for each excess fringe in the original interferograms, a phase singularity, which is the very centre of the vortex around which the phase winds M times. Note that a fork-like interference slit or a thickness varying plate can be both used also for the shaping of a photonic gaussian LG_{00} beam into a LG_{0M} Laguerre Gauss vortex beam, to be used for direct resonant imprint. Alternatively, space light modulators (SLM, cf. ref. [21]) or q-plate devices (patterned liquid crystal phase-retarder, see [22, 23, 24]) can be used with more versatility

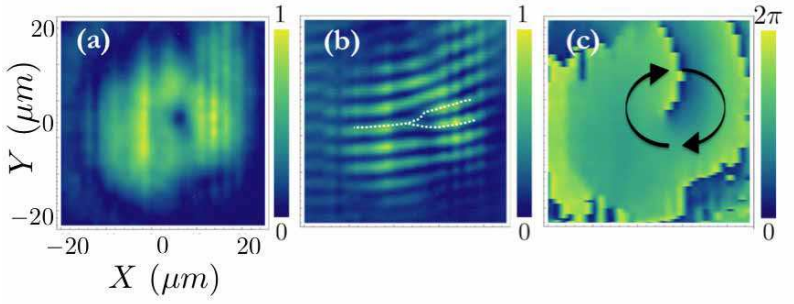

Figure 1.1 Figure taken from Ref. [20]. Panel (a) reports the space distribution of the intensity associated to the vortex state. When overlapped to a homogeneous wavefront of a coherent beam, the resulting interferogram shows a fork-like pattern as that of panel (b). The associated phase map retrieved by means of Fourier filtering is reported in panel (c), displaying a phase singularity with a $M = +1$ winding of the phase around the core.

to such an extent. For a more detailed explanation of time-resolved digital holography imaging in polariton fluids see [20, 25].

1.3 Polariton spinor nature and half-vortices

The polarization degree of freedom within photons coupled to the spin of excitons makes the polariton condensate a spinor quantum fluid, analogous two a two-component atomic BEC. This property allows to obtain a rich variety of topological excitations featuring different polarization patterns, as described in [13, 26, 27, 28]. All these states are analogous to purely photonic vectorial fields, apart from three main features typical for polaritons: strong nonlinearity, sample disorder landscape and symmetry breaking terms such as TE-TM or x-y splitting. Two main interesting states are possible when looking at a full basis of, say, right and left (R, L) polarization components. In the first case, usually referred to as a full-vortex (FV), a vortex with the same winding exists in both polarisations. This results in a fixed linear polarization with a integer winding of the phase. The second case is a vortex in only one spin population coupled to a Gaussian or homogeneous profile in the opposite spin population, and is usually referred to as a half-vortex, HV. Such term derives from the half-integer winding of both phase and linear polarization direction which is seen in a HV state, as illustrated in Figure 1.2.

Here the left and right panels show the cases of lemon and star half-

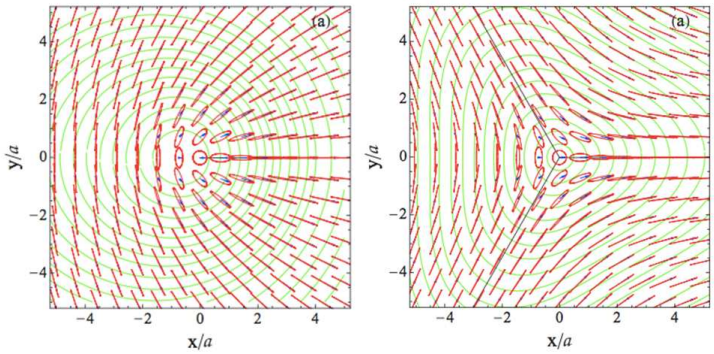

Figure 1.2 Figure taken from Ref. [28]. The two kind of half-vortices, lemon (left) and star (right), with their associated polarization patterns. At large distance from the centre, the polarization is linear and its direction makes a half-rotation when one moves around a space circumference.

vortices, respectively, which are associated to homologue or heterologue OAM and SAM directions. Nonresonant spontaneous generation or resonant imprinting of half-vortices are both possible, see in the following and the last sections.

1.4 Nonresonant excitation and spontaneous vortices

Several different observations of spontaneous vortices have been made in nonresonantly created polariton condensates. Initially, the first detection of spontaneous formation of pinned quantized vortices in the Bose-condensed phase of a polariton fluid, allowed to draw parallels between polariton systems and conventional BEC [12]. Subsequently, a coexistence of half-quantum vortices (HV) and single-quantum vortices (FV) was shown in microcavity polaritons, as expected for a spinor quantum fluid [13, 29]. In these cases Lagoudakis *et al.* showed the role of the landscape disorder in pinning one or the other of the two elementary states. This role was later confirmed by the dynamical imaging of the dissociation of a full-vortex into a pair of half-vortices [26], which also put into evidence the creation of different combination of elementary charges giving rise to patterns such as that of an hyperbolic vortex [27].

Recently, starting from a ring shaped potential, the formation of a different kind of a more generic half-vortices with the polarization winding spanning both linear and circular states [30] was observed. Inhomogeneous

spot profiles can be used to induce formation of a single vortex-antivortex pair [31], or of a lattice consisting of a few vortices [32], due to an interplay of phase-fluctuations and disorder pinning. Other non-homogeneous optical pump beams such as multiple spots can generate a lattice of many vortices, due to the locking of propagating flows over long area and their mutual interference [33]. A structured optical pump beam could also be used to induce the breaking of chiral symmetry, inducing transfer of orbital angular momentum and creation of a single exciton-polariton vortex (so called chiral polaritonic lenses, see [34]). In either cases, the role of nonlinearities are fundamental, in both driving the polaritonic flows out of the originally excited area and in locking their mutual phase.

The effect of spontaneous free-single or bound-pair vortices on the long-range-order coherence of a superfluid and their link to the BerezinskyKosterlitzThouless (BKT) transition were discussed in [35]. Spontaneous vortices under off-resonant pumping have been observed also in organic polariton condensates in a disordered landscape. Here fluctuating formation of vortices were highlighted thanks to single or few shots interferograms [36, 37].

1.5 OPO condensates with imprinted and spontaneous vortices

1.5.1 Vortices imprinted on OPO condensate

In this section we describe a method to excite a vortex in an OPO system. Figure 1.3(b) shows the real space image of the OPO signal recorded at pump power 3 times above the condensation threshold, P_{th}. The uniform spatial distribution of the emission indicates high quality of the studied microcavity sample with very weak disorder [38]. In order to create a vortex state in the OPO signal emission a weak continuous wave *im*-beam carrying OAM $M = +1$ is introduced (Figure 1.3(c)). The power of the *im*-beam is ~ 40 times less than that of the signal and its frequency is tuned in resonance with the signal frequency. As it is shown in Figure 1.3(d) under the application of the *im*-beam the spatial distribution of the signal is modified with a resultant well-defined dip of diameter (FWHM) $\approx 7\mu$m, (radius $\approx 3.5\mu$m (HWHM)) labeled A. The dip arises from a vortex imprinted on the condensate profile. This is demonstrated by measuring the spatial phase variation of the OPO condensate [12]. For this purpose the interference pattern between the signal image in Figure 1.3(d) and the image inverted around a central point of symmetry was recorded, so that the region of a vortex core (labelled A) interferes with the region B (see Figure 1.3(d)) where the phase is nearly

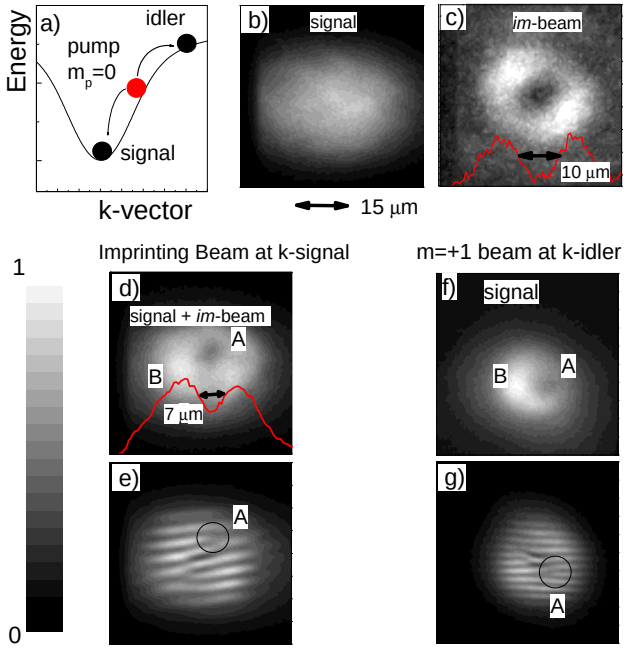

Figure 1.3 Figure taken from Ref. [18]. (a) Schematic diagram of OPO. (b) Real space image of the signal with no imprinting beam. (c) Image of Gauss-Laguerre imprinting beam (*im*-beam). (d) Signal with weak *im*-beam of (c), showing an imprinted vortex labeled A. (e) Interferogram revealing the 2π phase variation around the vortex of (d). (f) Vortex in signal, labeled A, created by excitation at the idler position with Gauss-Laguerre beam. (g) Interferogram revealing the vortex with OAM $M_s = -1$ created in (f). The red lines are cross-sections through the vortex cores of (c) to (d), with the sizes of the cores (FWHM) indicated.

constant. The resultant interference pattern shown in Figure 1.3(e) reveals the two fork-like dislocations, demonstrating formation of a single vortex in OPO signal state with OAM $M_s = 1$ around region A.

Since the *im*-beam is very weak it does not modify substantially the OPO signal population. However it changes spatial distribution of the phase of the OPO emission. Since the phase of the signal is undetermined in the OPO, the few polaritons injected by the *im*-beam lock the signal phase to their own. That is why the process above is described as "imprinting". We note, that experimentally a minimum ratio of the *im*-beam to signal power density of about $\sim 1/45$ is required to imprint a vortex in the OPO

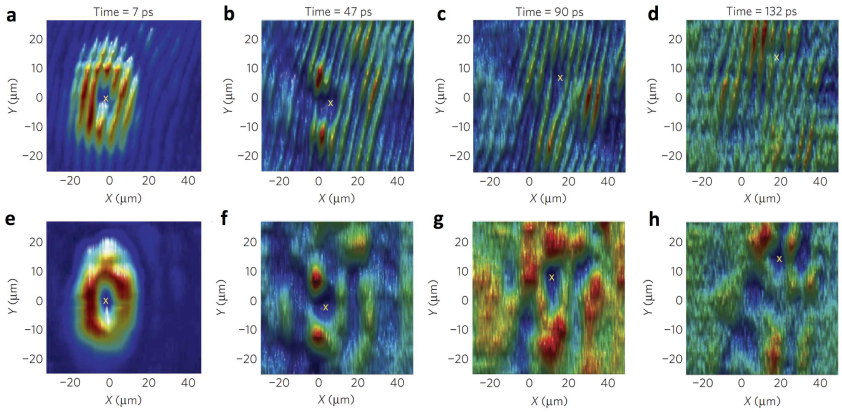

Figure 1.4 Dynamics of a vortex of angular momentum $M_s = 1$ imprinted into the signal steady state of a cw OPO signal. Four snapshots of the evolution of the vortex core at 7 ps, 47 ps, 90 ps and 132 ps after the probe pulse has arrived, are shown. In (a-d) the vortex core can be identified by the fork dislocation which is formed when the signal is made interfere with a constant wavefront taken from a spatial expanded part of the emission. In (e-h) the same images are shown in the intensity map. Figure taken from Ref. [41].

condensate. Decoherence processes occurring in polariton condensates due to fluctuations probably determine this limit [39, 40].

1.5.2 Temporal dynamics of a vortex imprinted on OPO polariton condensate

In another experiment [41] a picosecond laser pulse carrying OAM was employed to imprint a vortex state into the OPO signal steady state driven by a cw laser pump. The vortex behaviour with time was then tracked using a streak camera. The time evolution of an $M_s = 1$ vortex excited on top of the OPO signal and its interference pattern, which characterises unequivocally the vortex state, are shown in Figure 1.4. The external pulsed *im*-beam was set to have an intensity smaller than the signal state. In the sequence of Figure 1.4 it is possible to follow the vortex dynamics after the probe has generated it within the first few picoseconds. The vorticity, which was imprinted into the steady state of the signal, remains in the condensate for a time which is at least one order of magnitude longer than the polariton lifetime and is only limited by the time it takes to get out from the pump spot area. Such observation is a clear evidence that the quantum fluid of

polariton is behaving as a superfluid, showing frictionless rotation for times longer than the coherence time of the state: fringes, which show the typical fork like dislocation, disappear while the vortex core is still detectable in the intensity maps.

The formation of metastable rotating currents, in polariton fluids, showing the absence of scattering with defects (always present in microcavity samples), is consistent with the theoretical model of excitations in non-equilibrium polariton condensates [42]. This model predicts that perturbations created by defects are not able to propagate long distances due to finite damping rates of the excitations. As a result it is much harder to break the topological stability of the supercurrents.

The sample inhomogeneities, however, still play a significant role and are very useful in this experiment since they provide a deterministic path for the injected vortex that would otherwise undergo a random drift out of the injection spot. Such effect allows for the detection of the vortex dynamics which, contrarily would be washed out by the averaging over the many experimental realisations.

1.5.3 The effect of polariton-polariton interactions on vortex size

In Ref. [18] the effect of polariton-polariton interactions on the vortex size has been investigated. We note, that orbital angular momentum of light has been investigated in parametric down-conversion experiments [43], where the optical non-linearity has a $\chi^{(2)}$ form. By contrast, polariton-polariton interactions lead to the $\chi^{(3)}$ nonlinearity, which gives rise to OPO processes as well as to the blueshifts of polariton modes. As a result of these interactions the vortex size is determined by the healing length [44], a characteristic length scale within which a locally perturbed condensate wavefunction returns to its unperturbed value. In the case of a vortex the expression for the healing length of the OPO condensate $\xi \approx M_s(2m_{eff}\kappa n_s)^{-\frac{1}{2}}$ can be obtained by equating a typical kinetic energy associated with a vortex in the condensate, $\approx M_s^2(2m_{eff}\xi^2)^{-1}$ to the interaction energy (blueshift), which is $\approx \kappa n_s$ (all energies are scaled to $\hbar^2$). Here m_{eff} is the polariton effective mass, κ is the strength of the non-linearity, M_s is the value of OAM in the vortex, and n_s is the signal population density. Therefore, the healing length should scale with the number of particles as $n_s^{-0.5}$.

In order to investigate this population dependence the vortex radius in the OPO condensate was measured at different pump powers, which determine the density of particles in the signal. The real space images of the OPO condensate with an imprinted vortex are shown in Figures 1.5(a) and (b)

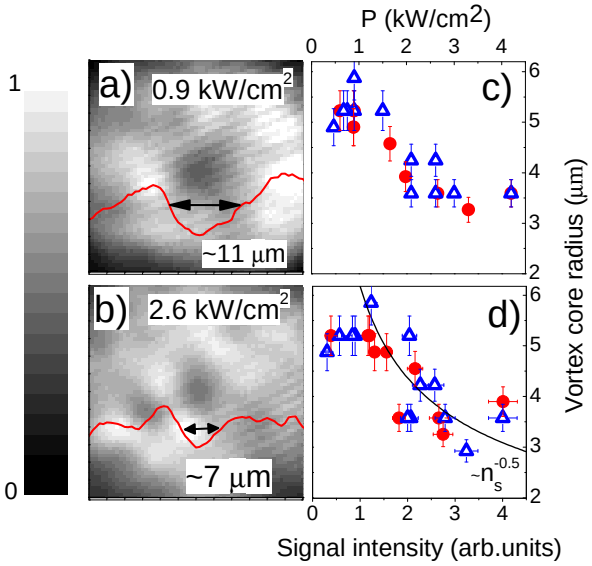

Figure 1.5 Figure taken from Ref. [18]. (a), (b) Images of a signal vortex at (a) 0.9 kWcm^{-2} and (b) 2.6 kWcm^{-2}. Experimental vortex core radius of the OPO signal as a function of pump power (c) and as a function of the signal intensity (d) for an *im*-beam core radius of $\sim 4\mu$m (circles) and $\sim 7\mu$m (triangles), respectively.

for pump powers P=$\sim$ $1.5P_{th}$ and P=$\sim$ $4.5P_{th}$, respectively. The vortex radius (healing length) apparently reduces with increasing signal particle density. The vortex core radius (Figure 1.5(c)) decreases from ~ 5.5 μm at threshold down to $\sim$ 3 μm at excitation density 5 times above threshold. Moreover, very similar variations of the vortex size with polariton density were observed for two different sizes of the *im*-beam, indicating that the profile of the imprinted vortex is an intrinsic property of the interacting polariton condensate. As is shown in Figure 1.5(d) the dependence of the vortex radius versus signal intensity scales approximately as $n_s^{-\frac{1}{2}}$ (solid line) in agreement with the expression for the healing length above. However, at small signal intensities the vortex radius does not diverge as expected from the $n_s^{-\frac{1}{2}}$, but is probably limited by the finite signal size.

Let's compare the magnitudes of the vortex radius in the polariton and atom systems: for polaritons, $m_{eff} \sim 10^{-5} m_e$, and $\kappa n_s \sim 10^{-1}$ meV. By contrast in a rubidium BEC with a density $n \sim 10^{14}$ cm^{-3} the effective mass of an atom is much larger $m_{eff} \sim 10^5 m_e$ than that of a polariton,

which is compensated by the much smaller interaction energy per single particle $gn = 4\pi a_s n\hbar^2/M \sim 10^{-7}$ meV where the atom scattering length $a_s \approx 5$ nm [44] and g is the atom interaction strength. As a result, the healing length for the polariton and the atom systems are of the order of 10 μm and 0.1 μm, respectively.

In the OPO system the vortex is imprinted onto the signal condensate, which arises due to polariton-polariton scattering from the pump into the signal and idler. If the pump state is driven by a laser with zero OAM, then conservation of OAM in the polariton-polariton scattering should dictate formation of an antivortex state with OAM $M_i = -1$ in the idler. It is difficult to directly image the idler state and hence to demonstrate the creation of an anti-vortex state, since the idler intensity is typically > 100 times weaker than that of the signal [40] due to the small photonic component of polariton states at high momenta. In order to demonstrate the conservation of OAM in the parametric scattering a seed laser beam with OAM $M_i = +1$ was applied at the angle and energy where the OPO idler would appear. The seed laser stimulates the pair polariton scattering from the pump with resultant formation of the 'signal' forming at $k \sim 0$. The signal state imaged in Figure 1.3(f) carriers an anti-vortex state with OAM $M_s = -1$ as is further confirmed by the corresponding self-interference image shown in Figure 1.3(g) [18].

1.5.4 Spontaneous vortices with OAM $M_s = 1$ in an OPO condensate using ring-shaped excitation

In this section we show that spontaneous vortices may also appear in the OPO condensates subject to optically shaped external potential due to polariton flow from high to low potential energy (and high to low gain) region. The OPO is excited using the ring-shaped pump, which is prepared by placing an opaque mask on the way of the Gaussian excitation laser beam [19]. As a result of such excitation the OPO condensate also has a ring-shaped profile as shown in Figure 1.6(c). The corresponding self interference pattern of the signal emission is shown in Figure 1.6(d), which exhibits clearly the fork-like dislocations indicating vortex formation with orbital angular momentum OAM $M_s = 1$ as in the case of imprinted vortex.

Polariton-polariton interactions, which are stronger in the high than in low density region, form an optically induced potential trap due to density-induced polariton blue-shifts. As a result, polaritons flow from high to low density region in the center of the pump spot acquiring kinetic energy and rotary motion with the resulant formation of a vortex state. The radius of the

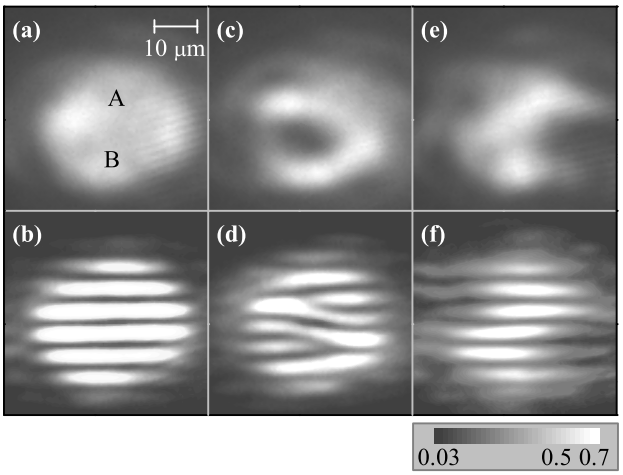

Figure 1.6 . Figure taken from Ref. [19].(a) is the spatial image of a uniform OPO condensate. (b) shows the interference pattern obtained by interfering the image with its inverted image and overlapping positions A and B. No fork, i.e. no vortex is observed. (c) shows the image of an ring shaped condensate, induced by a ring-shaped pump beam. The corresponding interference image (d) reveals a single spontaneous vortex inside the ring. (e) and (f) show the case where the mask was moved towards the edge of the beam and no vortex forms.

optical potential trap coincides with the typical vortex size (healing length) $\xi \sim 5$ μm [18] described by OAM $M_s = +1$ as discussed above. In this case the potential energy associated with repulsive interactions in the high density region ($\sim 0.1 - 0.2$ meV) is similar to the kinetic energy associated with the vortex in the low density region, making it more favourable for the condensate to form a stable single vortex. We note that an optical trap with well-defined boundaries is required for the spontaneous vortex to be formed: no vortices are observed if the opaque mask is moved close to the edge of the excitation spot as shown in Figures 1.6(e-f)

It is not very clear why a polariton condensate excited by a ring-shaped laser favors the vortex with a particular sign of OAM. Generally, the vortex states with OAM of both $M_s = 1$ and $M_s = -1$ are expected to be formed if the OPO system has $y \mapsto -y$ reflection symmetry perpendicular to the pump wave-vector (k_p, 0). An irregular doughnut shape of the pump spot can easily break this reflection symmetry which may result in a spontaneous formation of a vortex state with a particular sign of OAM. The results are consistent with the observation in Ref. [34], where a spontaneous vortex was observed in a polariton condensate excited by the spatially shaped chiral

pump beam, which also created an optically induced potential possessing no cylindrical and $y \mapsto -y$ reflection symmetry.

We note that Manni *et al.* [45] studied nonresonantly pumped condensates using ring-shaped excitation in CdTe microcavities and in contrast to the results here shown, observed a multi-lobe standing wave pattern, which is a coherent superposition of wavefunctions with OAMs $M_s = +1$ and $M_s = -1$. Their observation indicates the breaking of cylindrical but not of reflection symmetry. On the other hand, the reflection symmetry can be easily broken by some disorder potential across the sample and spontaneous vortices only with OAM $M = 1$ can be observed in the same CdTe based microcavities [12].

1.5.5 Observation of spontaneous vortex with OAM $M_s = 2$ in OPO condensate

In this section we explore the effect of the density dependent polariton interactions on the healing length in condensates using the ring shaped pump beam excitation. Figures 1.7(a-f) and shows real space density images of the OPO condensate and the corresponding interference patterns for increasing pump powers from 73 to 180 mW. The images in Figures 1.7(a, d) correspond to a power of $1.1P_{th} = 73$ mW, just above condensation threshold P_{th}. The formation of a vortex with OAM $M_s = 1$ can be observed. For increasing pump powers up to 150 mW the condensate keeps its ring-like shape and the vortex survives maintaining its charge of $M_s = 1$ (Figures 1.7(b, e)). However, a surprising change takes place for $P = 180$ mW (Figures 1.7(c, f)), when, besides an apparent increase of the core diameter, the fork-like dislocation develops an additional arm corresponding to the next quantized vortex state with OAM $M_s = 2$.

Figure 1.7(g) shows intensity profiles across the center of the vortex for varying pump intensities. The vortex core diameter (FWHM of the intensity profiles) vs pump power is shown in Figure 1.7(h). For increasing pump powers in the range of 70 to 150 mW the core diameter of the vortex changes slightly from about 13.5 μm down to 12 μm. However, a prominent jump of the core diameter to 16 μm occurs at 180 mW pump power and coincides with the transition from the vortex state with OAM $M_s = 1$ to the state with OAM $M_s = 2$. With increasing polariton population density the interaction energy of polaritons away from the vortex core also increases, which is, as discussed above, compensated by the increased kinetic energy of polaritons in the vortex core with resultant slight shrinking of the vortex size (healing length). However, in this experimental arrangement the OPO condensate

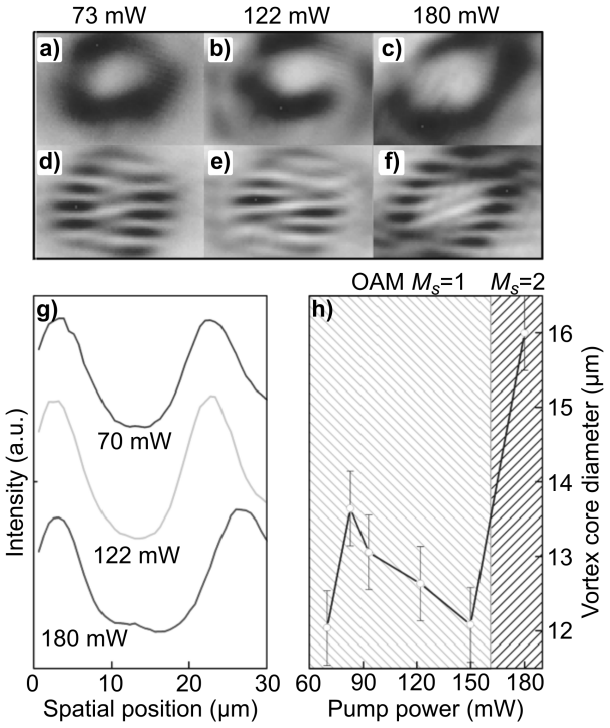

Figure 1.7 Spatial images of vortex with OAM $M_s = 1$ (a, b) and OAM $M_s = 2$ (c). (d, e, f) The interference patterns revealing vortex states with OAM $M_s = 1$ (d, e) and $M_s = 2$ (f). (g) Intensity profiles across the center of the vortex for varying pump intensities. (h) The vortex core diameter vs pump power.

is supported by the gain from the ring-shaped pump, which hence places a lower bound on the vortex core size (the pump density is almost zero in the middle of the pump spot). Therefore, it appears to be more favorable for the system to increase the kinetic energy by forming a higher order quantized vortex state with $M_s = 2$. As a result of such a transformation the healing length $\xi = M_s(2m_{eff}\kappa n_s)^{-\frac{1}{2}}$ also should increase abruptly in agreement with the experimental observation in Figure 1.7.

1.6 Dynamics of vortices in resonant polariton condensates

In this section we see that the versatility of the resonant excitation allows the direct imprint of a polariton condensate carrying a single, half or multiple

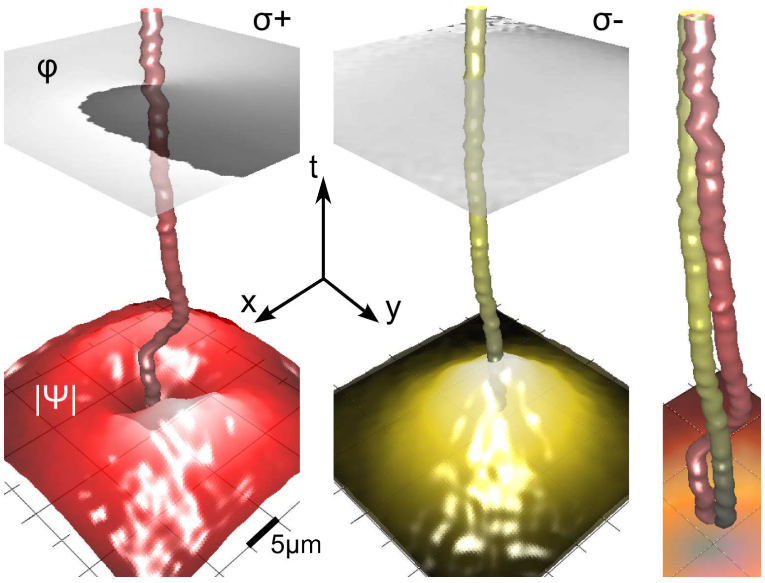

Figure 1.8 Figure elaborated from data of Ref. [22]. An half-vortex state is represented by means of its two spin components σ_+ and σ_-, on left and mid columns, respectively. The initial space distributions of the amplitude are reported in the bottom of the figure, while the phase maps appear in the top. The 2D+t strings represent the evolution of the phase singularity for the vortex component and of the maximum of the density for the gaussian one, in a 40 ps time range. Last panel puts into evidence a spiralling of the vortex core around the centroid of the opposite spin population.

vortices, in other terms, directly created with an integer non-zero OAM. Naturally, spontaneous couple-generation of secondary vortices is also possible within the resonant scheme, for example induced by using an inhomogeneous pump beam such as ring or multiple spots or by creating the fluid with a given finite-k and sending it against a defect.

In a fundamental configuration, the resonant scheme allows to generate a condensate directly carrying a single full or half vortex state as initial conditions [22]. The wavefronts of the photonic excitation pulse are shaped by a patterned phase retarder, in order to give Laguerre Gauss beams to be sent on the microcavity sample. A time resolved imaging of the polariton fluid is obtained thanks to delay line interferometry of the emission with a coherent and spatially homogeneous pulse. Each spin population of a full vortex, and only one spin component in the half vortex, carries a OAM = +1. Every phase singularity is then digitally tracked in time and their dynamics can be represented as 2D+t vortex strings/lines. The primary singularities (origi-

nal vortices), evolve due to an interplay of disorder landscape and nonlinear potential, which changes in time due to dissipation. An exemplificative case shows that the twin cores of a full vortex can undergo an erratic movement at low exciting densities (or at long times), and eventually separate each from the other under the action of a symmetry breaking term such as xy or TETM splitting. This is similar to what observed in the case of spontaneously formed vortices under nonresonant excitation scheme where disorder played a pivotal role [26]. At larger densities instead, the two main cores are seen to move together for longer times, while the nonlinear potential somehow screens the disorder potential out. Interspin interactions which are weak and attractive can supposedly help keeping the cores together. Another manifestation of them is that the singularity in an half vortex undergoes a spiralling trajectory around the density maximum of the opposite spin population, which acts as a gaussian trap in the case of a metastable rotating vortex, as predicted in [46], and experimentally reported in the example of Figure 1.8.

Instead, when a single polariton condensate is directly injected at $k = 0$ with an initial zero OAM, a inhomogeneous shape can be used to induce a fluid redistribution associated to radial currents. For example in [19] the

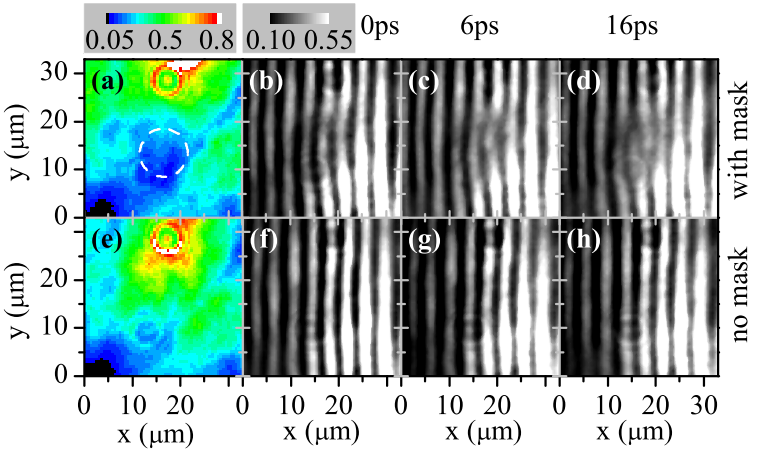

Figure 1.9 Taken from Ref.[[19]] Images of the transmitted beam with and without a 10 micron mask in the pump beam path are shown in (a), (e), respectively. A potential trap due to a lower polariton density is formed when the mask is present in the encircled area. (b-d) are interference images obtained with a reference pulse at $t = 0$, 6 and 16 ps and show the dynamics of the formation of a vortex-anti-vortex pair. (f)-(h) Without the potential trap, no vortex pair is formed.

condensate was excited with a pulsed laser beam focused into a large spot. A dip in the condensate background intensity was created by passing the beam through an opaque mask as above and the temporal dynamics of vortex formation due to polariton flows has been measured in such an optically induced potential. The detailed experimental arrangements are very similar to that in Ref. [16]. The real spatial image of the injected condensate is shown in Figure 1.6(a) with a dark region (encircled) created by the opaque mask. Figures 1.6(b-d) show the resultant interference patterns recorded as a function of time after the arrival of the excitation pulse. At time $t = 0$ the interference pattern indicates a nearly homogeneous phase distribution of the polariton field: no fork-like dislocations and hence no vortices are observed in the system. At later times the phase pattern becomes disturbed and then a vortex (V) - anti-vortex (AV) pair is clearly observed at about $t = 16$ ps (Figure 1.6(d)). These vortices arise from polariton flow to the low density region with small potential energy. Polaritons propagate at a typical speed of about ~ 1 μm/ps, which probably determines the timescale of V-AV formation. In this experimental arrangement, spontaneous vortices are always observed in V-AV pairs, but never as a single vortex, which is a consequence of the OAM conservation law. Since the polariton condensate was initially prepared in a state with OAM of $M = 0$ at $t = 0$, any spontaneous vortex with $M = 1$ arising from polariton flow should be accompanied by an anti-vortex [16, 17] with $M = -1$. In the OPO case studied in previous sections only single vortex states are observed in the signal, which is consistent with the fact that an antivortex state is created in the idler. Both vortex and anti-vortex states are possible in the OPO signal despite the presence of the idler, although this is not observed in our experiments. For example, a moving A-AV pair was observed in a spatially extended OPO signal perturbed with a probe pulse beam carrying an OAM of $M_s = 1$ [47].

In a different configuration, when the fluid is resonatly injected with a cw finite-k and sent to hit a localized defect (e.g., photonic point-like defect), the hydrodynamics regime changes upon density, passing from a superfluid state without turbulence to the formation of oblique dark solitons and vortex streets in the wake of the potential barrier [17]. The similar emission of vortex-anti-vortex pairs from a localized defect could be observed also under pulsed pumping, by ultrafast imaging of their transient dynamics [16]. Also lattices of vortex induced by resonant multiple-spot interference were theoretically studied, together with the stabilizing effects of nonlinearities, [48, 49] and experimentally realized by use of a mask-shaped potential [50], somehow analogously to what reported for the lattices described in the non-resonant section. Recently even an annular chain of co-winding vortices were

resonantly injected and their evolution in the linear and nonlineare regime experimentally explored [51].

1.7 Conclusion

To conclude, the polariton OPO supports a novel topological excitation consisting of a vortex in the signal and an anti-vortex in the idler. We have shown that the core radius of vortices in the polariton condensate is determined by polariton-polariton interactions. With ultra-fast measurement techniques the imprinting method also provides a means to investigate vortex dynamics on time-scales inaccessible in other systems. Metastable rotational polariton flow is observed indicating superfluid like behaviour of the nonequilibrium condensate. The spontaneous formation of quantized vortices in OPO polariton condensates is also observed in an optically induced ring-shaped potential trap. A transition from a vortex state with OAM $M_s = 1$ to one with $M_s = 2$ is observed in OPO condensates driven by a ring-shaped pump, which inhibits shrinking of the vortex size with power density and makes it more favourable for the system to switch to the state with higher OAM. In the case of a polariton population directly injected resonantly at $k = 0$ by a pump pulse a pair of vortices with OAM of opposite sign can develop, which preserves the initial injected OAM of $M = 0$. This excludes the observation of single vortices for such configuration. Neverthless, the versatility of coherent scheme allows also the direct excitation of both a single full- or half-vortex spinor condensate, and to follow their dynamics during the lifetime of polaritons, devising the interplay of nonlinearity, disorder, symmetry splitting terms and dissipation rates.

We acknowledge support by EPSRC grants EP/G001642 and EP/J007544. DS and LD acknowldege support from the ERC project POLAFLOW.

References

[1] V.Timofeev, and D.Sanvitto. 2012. *Exciton polariton in microcavities: New Frontiers, Springer Series in Solid-State*. Berlin, Germany: Springer.

[2] A. Kavokin, J. Baumberg, G. Malpuech, and Laussy, F. *Microcavities*. Oxford, UK: Oxford University Press.

[3] Wouters, Michiel, and Carusotto, Iacopo. 2007. Excitations in a Nonequilibrium Bose-Einstein Condensate of Exciton Polaritons. *Phys. Rev. Lett.*, **99**, 140402.

[4] Stevenson, R. M., Astratov, V. N., Skolnick, M. S., Whittaker, D. M., Emam-Ismail, M., Tartakovskii, A. I., Savvidis, P. G., Baumberg, J. J., and Roberts,

J. S. 2000. Continuous Wave Observation of Massive Polariton Redistribution by Stimulated Scattering in Semiconductor Microcavities. *Phys. Rev. Lett.*, **85**, 3680–3683.

[5] Tartakovskii, A. I., Krizhanovskii, D. N., and Kulakovskii, V. D. 2000. Polariton-polariton scattering in semiconductor microcavities: Distinctive features and similarities to the three-dimensional case. *Phys. Rev. B*, **62**, R13298–R13301.

[6] Wouters, Michiel, and Carusotto, Iacopo. 2007. Goldstone mode of optical parametric oscillators in planar semiconductor microcavities in the strong-coupling regime. *Phys. Rev. A*, **76**, 043807.

[7] Cross, M. C., and Hohenberg, P. C. 1993. Pattern formation outside of equilibrium. *Rev. Mod. Phys.*, **65**, 851–1112.

[8] Sigurdsson, H., Egorov, O. A., Ma, X., Shelykh, I. A., and Liew, T. C. H. 2014. Information processing with topologically protected vortex memories in exciton-polariton condensates. *Phys. Rev. B*, **90**, 014504.

[9] Matthews, M. R., Anderson, B. P., Haljan, P. C., Hall, D. S., Wieman, C. E., and Cornell, E. A. 1999. Vortices in a Bose-Einstein Condensate. *Phys. Rev. Lett.*, **83**, 2498–2501.

[10] Vinen, W. F. 1961. The Detection of Single Quanta of Circulation in Liquid Helium II. *Proc. R. Soc. Lond*, **260**, 218.

[11] Scheuer, J., and Orenstein, M. 1999. Optical Vortices Crystals: Spontaneous Generation in Nonlinear Semiconductor Microcavities. *Science*, **285**(5425), 230–233.

[12] K. G. Lagoudakis, M. Wouters, M. Richard A. Baas I. Carusotto R. Andre L. S. Dang, and Deveaud-Pledran, B. 2008. Quantized vortices in an exciton-polariton condensate. *Nat. Phys.*, **4**, 706.

[13] Lagoudakis, K. G., Ostatnický, T., Kavokin, A. V., Rubo, Y. G., André, R., and Deveaud-Plédran, B. 2009. Observation of Half-Quantum Vortices in an Exciton-Polariton Condensate. *Science*, **326**(5955), 974–976.

[14] M. Sich, D. N. Krizhanovskii, M. S. Skolnick A. V. Gorbach R. Hartley D. V. Skryabin E. A. Cerda-Méndez K. Biermann R. Hey P. V. Santos. 2012. Observation of bright polariton solitons in a semiconductor microcavity. *Nat. Photonics*, **6**, 50–55.

[15] Sich, M., Fras, F., Chana, J. K., Skolnick, M. S., Krizhanovskii, D. N., Gorbach, A. V., Hartley, R., Skryabin, D. V., Gavrilov, S. S., Cerda-Méndez, E. A., Biermann, K., Hey, R., and Santos, P. V. 2014. Effects of Spin-Dependent Interactions on Polarization of Bright Polariton Solitons. *Phys. Rev. Lett.*, **112**, 046403.

[16] G. Nardin, G. Grosso, Y. Leger B. Petka F. Morier-Genoud, and Deveaud-Plédran, B. 2011. Hydrodynamic nucleation of quantized vortex pairs in a polariton quantum fluid. *Nat. Phys.*, **7**, 635.

[17] Amo, A., Pigeon, S., Sanvitto, D., Sala, V. G., Hivet, R., Carusotto, I., Pisanello, F., Leménager, G., Houdré, R., Giacobino, E, Ciuti, C., and Bramati, A. 2011. Polariton Superfluids Reveal Quantum Hydrodynamic Solitons. *Science*, **332**(6034), 1167–1170.

[18] Krizhanovskii, D. N., Whittaker, D. M., Bradley, R. A., Guda, K., Sarkar, D., Sanvitto, D., Vina, L., Cerda, E., Santos, P., Biermann, K., Hey, R., and Skolnick, M. S. 2010. Effect of Interactions on Vortices in a Nonequilibrium Polariton Condensate. *Phys. Rev. Lett.*, **104**, 126402.

[19] Guda, K., Sich, M., Sarkar, D., Walker, P. M., Durska, M., Bradley, R. A., Whittaker, D. M., Skolnick, M. S., Cerda-Méndez, E. A., Santos, P. V., Biermann, K., Hey, R., and Krizhanovskii, D. N. 2013. Spontaneous vortices in optically shaped potential profiles in semiconductor microcavities. *Phys. Rev. B*, **87**, 081309.

[20] Antón, C., Tosi, G., Martín, M. D., Viña, L., Lemaître, A., and Bloch, J. 2012. Role of supercurrents on vortices formation in polariton condensates. *Opt. Express*, **20**(15), 16366.

[21] Dreismann, Alexander, Cristofolini, Peter, Balili, Ryan, Christmann, Gabriel, Pinsker, Florian, Berloff, Natasha G., Hatzopoulos, Zacharias, Savvidis, Pavlos G., and Baumberg, Jeremy J. 2014. Coupled counterrotating polariton condensates in optically defined annular potentials. *Proc. Natl. Acad. Sci.*, **111**(24), 8770–8775.

[22] Dominici, L., Dagvadorj, G., Fellows, J. M., Donati, S., Ballarini, D., De Giorgi, M., Marchetti, F. M., Piccirillo, B., Marrucci, L., Bramati, A., Gigli, G., Szymaska, M. H., and Sanvitto, D. 2014. Vortex and half-vortex dynamics in a spinor quantum fluid of interacting polaritons. *arXiv*, **1403.0487**.

[23] D'Ambrosio, Vincenzo, Baccari, Flavio, Slussarenko, Sergei, Marrucci, Lorenzo, and Sciarrino, Fabio. 2015. Arbitrary, direct and deterministic manipulation of vector beams via electrically-tuned q-plates. *Sci. Rep.*, **5**.

[24] Cardano, Filippo, Karimi, Ebrahim, Marrucci, Lorenzo, de Lisio, Corrado, and Santamato, Enrico. Generation and dynamics of optical beams with polarization singularities. *Opt. Express*, **21**(7), 8815–8820.

[25] Dominici, L., Colas, D., Donati, S., Cuartas, J. P. Restrepo, Giorgi, M. De, Ballarini, D., Guirales, G., Carreño, J. C. Lopez, Bramati, A., Gigli, G., del Valle, E., Laussy, F. P., and Sanvitto, D. 2014. Ultrafast Control and Rabi Oscillations of Polaritons. *Phys. Rev. Lett*, **113**, 226401.

[26] Manni, F, Lagoudakis, KG, and Liew, T C H. 2012. Dissociation dynamics of singly charged vortices into half-quantum vortex pairs. *Nat. Commun.*, **3**, 1309.

[27] Manni, F., Léger, Y., Rubo, Y. G., André, R., and Deveaud, B. 2013. Hyperbolic spin vortices and textures in exciton-polariton condensates. *Nat. Commun.*, **4**.

[28] Toledo-Solano, M., Mora-Ramos, M. E., Figueroa, A., and Rubo, Y. G. 2014. Warping and interactions of vortices in exciton-polariton condensates. *Phys. Rev. B*, **89**, 035308.

[29] Lagoudakis, K. G., Manni, F., Pietka, B., Wouters, M., Liew, T. C. H., Savona, V., Kavokin, A. V., André, R., and Deveaud-Plédran, B. 2011. Probing the Dynamics of Spontaneous Quantum Vortices in Polariton Superfluids. *Phys. Rev. Lett.*, **106**, 115301.

[30] Liu, Gangqiang, Snoke, David W., Daley, Andrew, Pfeiffer, Loren N., and West, Ken. 2015. A new type of half-quantum circulation in a macroscopic polariton spinor ring condensate. *Proc. Natl. Acad. Sci.*, **112**(9), 2676–2681.

[31] Roumpos, Georgios, Fraser, Michael D, Loffler, Andreas, Hofling, Sven, Forchel, Alfred, and Yamamoto, Yoshihisa. 2011. Single vortex-antivortex pair in an exciton-polariton condensate. *Nat. Phys.*, **7**(2), 129–133.

[32] Manni, F., Liew, T. C. H., Lagoudakis, K. G., Ouellet-Plamondon, C., André, R., Savona, V., and Deveaud, B. 2013. Spontaneous self-ordered states of vortex-antivortex pairs in a polariton condensate. *Phys. Rev. B*, **88**, 201303.

[33] Tosi, G, Christmann, G, Berloff, N G, Tsotsis, P, Gao, T, Hatzopoulos, Z, Savvidis, P G, and Baumberg, J J. 2012. Geometrically locked vortex lattices in semiconductor quantum fluids. *Nat. Commun.*, **3**, 1243.

[34] Dall, Robert, Fraser, Michael D., Desyatnikov, Anton S., Li, Guangyao, Brodbeck, Sebastian, Kamp, Martin, Schneider, Christian, Höfling, Sven, and Ostrovskaya, Elena A. 2014. Creation of Orbital Angular Momentum States with Chiral Polaritonic Lenses. *Phys. Rev. Lett.*, **113**, 200404.

[35] Nitsche, Wolfgang H., Kim, Na Young, Roumpos, Georgios, Schneider, Christian, Kamp, Martin, Höfling, Sven, Forchel, Alfred, and Yamamoto, Yoshihisa. 2014. Algebraic order and the Berezinskii-Kosterlitz-Thouless transition in an exciton-polariton gas. *Phys. Rev. B*, **90**, 205430.

[36] Plumhof, Johannes D, Stöferle, Thilo, Mai, Lijian, Scherf, Ullrich, and Mahrt, Rainer F. 2014. Room-temperature BoseEinstein condensation of cavity exciton-polaritons in a polymer. *Nat. Mater.*, **13**(3), 247–252.

[37] Daskalakis, Konstantinos S., Maier, Stefan A., and Kéna-Cohen, Stéphane. 2015. Spatial coherence and stability in a disordered organic polariton condensate. *arXiv*, **1503.01373**.

[38] Tinkler, L., Walker, P. M., Clarke, E., Krizhanovskii, D. N., Bastiman, F., Durska, M., and Skolnick, M. S. 2015. Design and characterization of high optical quality InGaAs/GaAs/AlGaAs-based polariton microcavities. *Appl. Phys. Lett.*, **106**, 021109.

[39] Love, A. P. D., Krizhanovskii, D. N., Whittaker, D. M., Bouchekioua, R., Sanvitto, D., Rizeiqi, S. Al, Bradley, R., Skolnick, M. S., Eastham, P. R., André, R., and Dang, Le Si. 2008. Intrinsic Decoherence Mechanisms in the Microcavity Polariton Condensate. *Phys. Rev. Lett.*, **101**, 067404.

[40] Krizhanovskii, D. N., Sanvitto, D., Love, A. P. D., Skolnick, M. S., Whittaker, D. M., and Roberts, J. S. 2006. Dominant Effect of Polariton-Polariton Interactions on the Coherence of the Microcavity Optical Parametric Oscillator. *Phys. Rev. Lett.*, **97**, 097402.

[41] D. Sanvitto, F. M. Marchetti, M. H. Szymaska G. Tosi-M. Baudisch F. P. Laussy D. N. Krizhanovskii M. S. Skolnick L. Marrucci A. Lemaitre J. Bloch C. Tejedor L. Vina. 2010. Persistent currents and quantized vortices in a polariton superfluid. *Nat. Phys.*, **6**, 527533.

[42] Wouters, Michiel, and Carusotto, Iacopo. 2010. Superfluidity and Critical Velocities in Nonequilibrium Bose-Einstein Condensates. *Phys. Rev. Lett.*, **105**, 020602.

[43] Martinelli, M., Huguenin, J. A. O., Nussenzveig, P., and Khoury, A. Z. 2004. Orbital angular momentum exchange in an optical parametric oscillator. *Phys. Rev. A*, **70**, 013812.

[44] Pitaevskii, L. P., and Stringari, S. 2003. *Bose–Einstein Condensation*. Oxford, UK: Clarendon Press.

[45] Manni, F., Lagoudakis, K. G., Liew, T. C. H., André, R., and Deveaud-Plédran, B. 2011. Spontaneous Pattern Formation in a Polariton Condensate. *Phys. Rev. Lett.*, **107**, 106401.

[46] Ostrovskaya, Elena A., Abdullaev, Jasur, Desyatnikov, Anton S., Fraser, Michael D., and Kivshar, Yuri S. 2012. Dissipative solitons and vortices in polariton Bose-Einstein condensates. *Phys. Rev. A*, **86**(1), 013636.

[47] Tosi, G., Marchetti, F. M., Sanvitto, D., Anton, C., Szymanska, M. H., Berceanu, A., Tejedor, C., Marrucci, L., Lemaitre, A., Bloch, J., and Vina,

L. 2011. Onset and Dynamics of Vortex-Antivortex Pairs in Polariton Optical Parametric Oscillator Superfluids. *Phys. Rev. Lett.*, **107**, 036401.

[48] Liew, T. C. H., Rubo, Yuri G., and Kavokin, A. V. 2008. Generation and Dynamics of Vortex Lattices in Coherent Exciton-Polariton Fields. *Phys. Rev. Lett.*, **101**, 187401.

[49] Gorbach, A. V., Hartley, R., and Skryabin, D. V. 2010. Vortex Lattices in Coherently Pumped Polariton Microcavities. *Phys. Rev. Lett.*, **104**, 213903.

[50] Hivet, R., Cancellieri, E., Boulier, T., Ballarini, D., Sanvitto, D., Marchetti, F. M., Szymanska, M. H., Ciuti, C., Giacobino, E., and Bramati, A. 2014. Interaction-shaped vortex-antivortex lattices in polariton fluids. *Phys. Rev. B*, **89**, 134501.

[51] Boulier, T, Terças, H, Solnyshkov, D D, Glorieux, Q, Giacobino, E, Malpuech, G, and Bramati, A. 2015. Vortex Chain in a Resonantly Pumped Polariton Superfluid. *Sci. Rep.*, **5**.